

## Speckle-dependent accuracy in phase-sensitive optical coherence tomography: supplement

**MATT S. HEPBURN,<sup>1,2,\*</sup>  KEN Y. FOO,<sup>1,2</sup>  PHILIP WIJESINGHE,<sup>1,3</sup>  PETER R. T. MUNRO,<sup>2,4</sup>  LIXIN CHIN,<sup>1,2</sup> AND BRENDAN F. KENNEDY<sup>1,2,5</sup>**

<sup>1</sup>*BRITElab, Harry Perkins Institute of Medical Research, QEII Medical Centre, Nedlands, Western Australia, 6009, Australia and Centre for Medical Research, The University of Western Australia, Crawley, Western Australia, 6009, Australia*

<sup>2</sup>*Department of Electrical, Electronic & Computer Engineering, School of Engineering, The University of Western Australia, 35, Stirling Highway, Perth, Western Australia, 6009, Australia*

<sup>3</sup>*Current address: SUPA, School of Physics and Astronomy, University of St. Andrews, KY16 9SS, UK*

<sup>4</sup>*Department of Medical Physics and Biomedical Engineering, University College London, Gower Street, London WC1E 6BT, UK*

<sup>5</sup>*Australian Research Council Centre for Personalised Therapeutics Technologies, Australia*

\*[matt.hepburn@research.uwa.edu.au](mailto:matt.hepburn@research.uwa.edu.au)

---

This supplement published with The Optical Society on 17 May 2021 by The Authors under the terms of the [Creative Commons Attribution 4.0 License](https://creativecommons.org/licenses/by/4.0/) in the format provided by the authors and unedited. Further distribution of this work must maintain attribution to the author(s) and the published article's title, journal citation, and DOI.

Supplement DOI: <https://doi.org/10.6084/m9.figshare.14381690>

Parent Article DOI: <https://doi.org/10.1364/OE.417954>

# Supplementary material to: Speckle-dependent accuracy in phase-sensitive optical coherence tomography

**MATT S. HEPBURN,<sup>1,2\*</sup> KEN Y. FOO,<sup>1,2</sup> PHILIP WIJESINGHE,<sup>1,3</sup>  
PETER R. T. MUNRO,<sup>2,4</sup> LIXIN CHIN,<sup>1,2</sup> AND  
BRENDAN F. KENNEDY,<sup>1,2,5</sup>**

<sup>1</sup>*BRITElab, Harry Perkins Institute of Medical Research, QEII Medical Centre, Nedlands, Western Australia, 6009, Australia and Centre for Medical Research, The University of Western Australia, Crawley, Western Australia, 6009, Australia*

<sup>2</sup>*Department of Electrical, Electronic & Computer Engineering, School of Engineering, The University of Western Australia, 35, Stirling Highway, Perth, Western Australia, 6009, Australia*

<sup>3</sup>*Current address: SUPA, School of Physics and Astronomy, University of St. Andrews, KY16 9SS, UK*

<sup>4</sup>*Department of Medical Physics and Biomedical Engineering, University College London, Gower Street, London WC1E 6BT, UK*

<sup>5</sup>*Australian Research Council Centre for Personalised Therapeutics Technologies, Australia*

*\*matt.hepburn@research.uwa.edu.au*

© 2021 Optical Society of America under the terms of the [OSA Open Access Publishing Agreement](#)

## 1. Speckle bias characterization

In Fig. S1, we demonstrate that the inaccuracy in phase difference from speckle is unbiased by comparing the mean value of many experimental measurements between a specular reflector and a scattering phantom. As described in Section 2.1, speckle introduces a fundamental inaccuracy to phase difference measurements. Importantly, this inaccuracy is dependent on the degree of local interference. In practice, whilst the distribution of scatterers in a turbid sample is deterministic, the location of each scatterer can be considered randomly distributed. As described in Section 2.1, consistent with existing literature, phase difference measured in a specular reflector is unbiased [1,2]. Therefore, we use the mean value of many phase difference measurements acquired in a specular reflector (provided by a polished mirror) with a high OCT SNR as an approximation to the true phase difference. For an equivalent translation between a specular reflector and speckle, this true phase difference can be used to analyze whether phase difference measured in speckle is unbiased.

The experimental setup is described in Section 3 of the main paper. To ensure the translation is equivalent between the two cases, we first set the voltage applied to the actuator and acquire an  $(x,z)$  complex OCT B-scan pair of the mirror. Without changing the system, the mirror was removed and replaced with the scattering phantom. An  $(x,z)$  complex OCT B-scan pair of the scattering phantom was then acquired. We applied an arbitrary translation of  $0.325\ \mu\text{m}$  (equivalent to a  $\pi$  radians phase shift) in both cases. For both cases, we acquire one B-scan pair and calculate the phase difference between B-scans acquired at different translation levels in each pair. Phase difference is calculated between pixels at the same location. Regions of the OCT SNR and phase difference  $(x,z)$  B-scan of the specular reflector that were analyzed in this section are shown in Figs. S1(a) and S1(b), respectively. The mean of 200 phase difference measurements,  $\mu_{\Delta\phi}$ , acquired at a constant depth along the  $x$ -dimension in a region of high OCT SNR in the specular reflector was  $\sim 2.406$  radians. The effective SNR [3] in this case was  $\sim 43$  dB. As the system was unchanged between both samples, this value is taken to be the true phase difference applied in each case.

Regions of the OCT SNR and phase difference  $(x,z)$  B-scans of the scattering phantom that were analyzed are shown in Figs. S1(c) and S1(d), respectively. In Fig. S1(c), speckle is clearly visible in the OCT SNR. A histogram of 200 phase difference measurements acquired

in independent speckle realizations at a constant depth along the  $x$ -dimension in the scattering phantom is shown in Fig. S1(e). The effective SNR in this case was  $\sim 21$  dB. The mean of these phase difference measurements was  $\sim 2.435$  radians. Here, the difference in translation measured between the two cases is approximately 3 nm, which is below the displacement sensitivity of the system at 20 dB ( $\sim 10$  nm). These results demonstrate that the phase difference measured across multiple speckle realizations, *i.e.*, the inaccuracy in speckle, is unbiased.

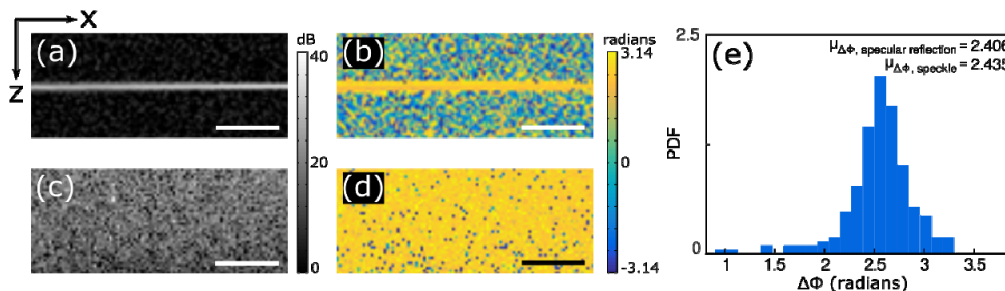


Fig. S1: (a) OCT SNR and (b) phase difference B-scans of a specular reflector. (c) OCT SNR and (d) phase difference B-scans of a scattering phantom. (e) Histogram of 200 phase difference measurements acquired at a constant depth from the center of the B-scan in the scattering phantom in (d). Scale bars represent  $500 \mu\text{m}$ .

## 2. Speckle brightness metrics

In this section, we describe two different methods of quantifying the amount of constructive interference of the OCT signal in speckle. As described in Section 2, speckle brightness, *i.e.*, the amount of constructive interference in the OCT signal, influences phase difference accuracy and sensitivity. As described in Section 3.3, an intuitive approach to measure speckle brightness is to compare the measured OCT amplitude to the maximum possible amplitude at each spatial location. This is illustrated in Fig. S2(a) for the case of a one-dimensional (1-D) simulation of an OCT A-scan. Details of the simulation are provided in Sections 2.1 and 3.1 of the main paper. Here, to demonstrate the principle of measuring speckle brightness, we analyze the OCT amplitude in the absence of optical noise. Figure S2(a) shows an arbitrary distribution of scatterers in depth. We simulate an OCT A-scan by convolving the distribution of scatterers with the complex point-spread function (PSF), where the real (blue line) and imaginary (green line) components of the complex OCT signal at each depth are shown. In addition, we plot the envelope (red line), equivalent to the OCT amplitude, of the complex OCT signal. As indicated by the arrows in Fig. 2(a), regions of constructive interference (bright speckle), and destructive interference (dark speckle) are clearly visible in this A-scan. The maximum OCT amplitude is determined in simulation by convolving the scatterers with the OCT point-spread function (PSF) envelope (dotted black line), *i.e.*, by ignoring the phase of the constituent responses.

Here, speckle brightness is quantified by dividing the measured OCT amplitude by the maximum possible amplitude which yields a measure from 0 (darkest speckle) to 1 (brightest speckle). We term this speckle brightness metric, *metric one* ( $M1$ ). The corresponding values of  $M1$  at each location for the simulation in Fig. S2(a) are shown in Fig. S2(b). Whilst  $M1$  provides a direct measure of speckle brightness, it is impractical in experiment as it requires prior knowledge of the precise location and reflectivity of each sub-resolution scatterer. Therefore, to quantify the degree of interference in experiment, we instead propose a metric based on the normalized Rayleigh distribution which is described in Section 3.3 of the main paper. We term the speckle brightness metric based on the Rayleigh distribution, *metric two* ( $M2$ ). Whilst  $M2$  does not provide a direct measure of speckle brightness, it has the advantage of only requiring the total OCT signal, and hence can be applied in experiment where the

exact locations and reflectivity of the sample scatterers are unknown. Importantly, both M1 and M2, can be applied in simulation, which can be used to assess the validity of M2.

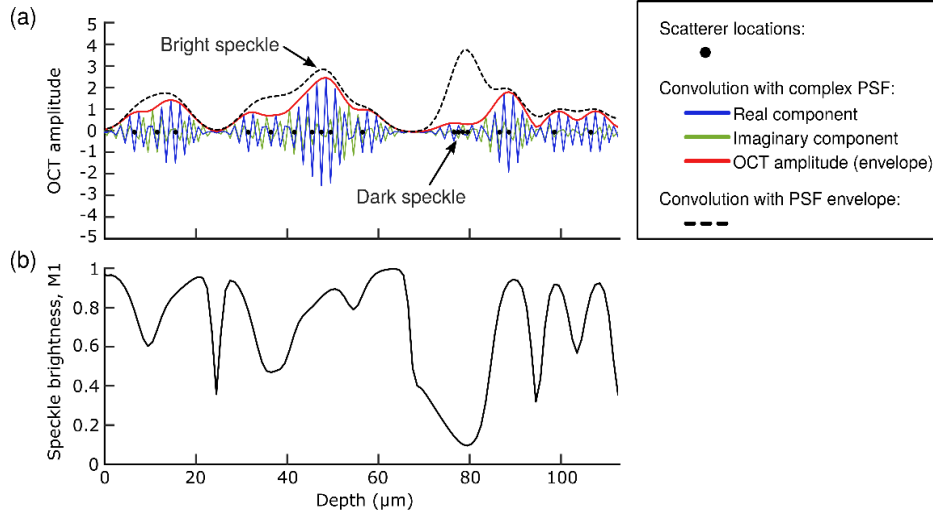


Fig. S2: Quantifying the constructive interference of the OCT signal in speckle. (a) Simulation of an OCT A-scan showing both the 1-D complex point-spread function, and 1-D point-spread function envelope, convolved with a distribution of scatterers in depth. (b) Corresponding speckle brightness using the M1 metric.

In Fig. S3, we compare the relationship between phase difference sensitivity and speckle brightness using both metrics in simulation. 255 million phase difference measurements are analyzed in Fig. S3 and Fig. S4. In Fig. S3, we translate the homogenous phantom  $1.3 \mu\text{m}$ , corresponding to a  $4\pi$  phase difference and compare points with the same OCT SNR and different values of speckle brightness. Note that M1 is in the range  $[0, 1]$ , whereas M2 is theoretically in the range  $[0, \infty]$ , and practically  $[0, 5]$ . Details of the simulation parameters, including the values used for optical noise and attenuation, are provided in Sections 2.1 and 3.1. In Figs. S3(a), S3(b), and S3(c), we present histograms of phase difference versus M1 for points with an SNR of  $15 \pm 1 \text{ dB}$ ,  $20 \pm 1 \text{ dB}$ , and  $25 \pm 1 \text{ dB}$ , respectively. Similarly, in Figs. S3(d), S3(e), and S3(f), we present histograms of phase difference versus M2 for points with an SNR of  $15 \pm 1 \text{ dB}$ ,  $20 \pm 1 \text{ dB}$ , and  $25 \pm 1 \text{ dB}$ , respectively. The color scale in Fig. S3 represents the number of measurements in each histogram bin divided by the total number of measurements. Here, both metrics are in close agreement, and in each case, the distribution of phase difference decreases in width for increasing speckle brightness.

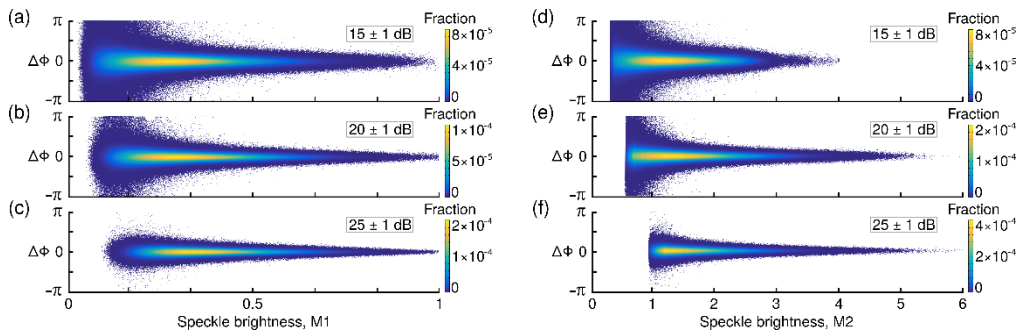


Fig. S3: Histograms of phase difference versus speckle brightness for points with an SNR of  $15 \pm 1 \text{ dB}$ ,  $20 \pm 1 \text{ dB}$ , and  $25 \pm 1 \text{ dB}$  using speckle brightness, M1 (a)–(c), and speckle brightness, M2 (d)–(f) for a fixed translation of  $1.3 \mu\text{m}$  ( $\Delta\phi = 4\pi$  radians).

Furthermore, in Fig. S4, we show the correlation between M1 and M2 by plotting the speckle brightness measured at each corresponding location using both metrics. The 45-degree line (dotted black line) represents a 1:1 correlation. The color scale in Fig. S4 represents the number of measurements in each histogram bin divided by the total number of measurements. Figure S4 shows a positive correlation (correlation coefficient of  $\sim 0.75$ ) between M1 and M2, which along with the results in Fig. S3, demonstrates that both metrics can be used to characterize the relationship between speckle brightness and phase difference sensitivity.

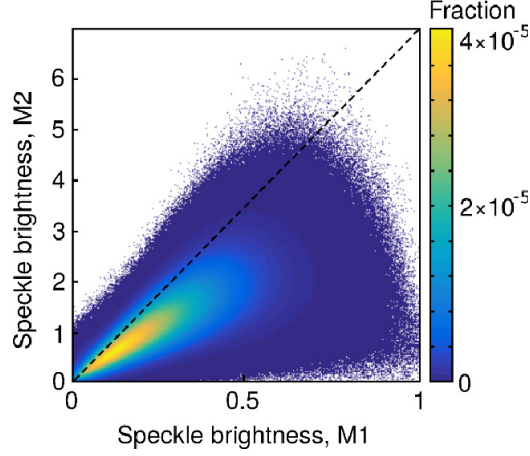


Fig. S4: A comparison between the speckle brightness metrics used in simulation (M1) and experiment (M2).

### 3. Averaging method

Here, we describe the method used to compute the mean OCT amplitude, OCT SNR and phase difference B-scans presented in Section 4. As described in Section 3.2 of the main paper, we acquire  $N$  B-scan pairs at each lateral  $y$ -location. Each B-scan pair consists of one complex OCT amplitude B-scan acquired with the sample under the static preload (referred to as the unloaded scan), and one complex OCT amplitude B scan acquired with an additional microscale compression loading (referred to as the loaded scan). For temporal averaging, we acquire  $N$  B-scan pairs at one lateral  $y$ -location. For spatial averaging, we acquire one B-scan pair at  $N$  lateral  $y$ -locations. In Sections 4.3 and 4.4,  $N = 100$ , and each B-scan pair in the spatially averaging case was acquired  $10 \mu\text{m}$  apart. We use the same method to compute the mean amplitude, OCT SNR, and phase difference in both the temporal and spatial averaging cases which is described below.

Firstly, we separate the unloaded and loaded complex OCT amplitude B-scans,  $A$ , from each B-scan pair. The complex intensity,  $I$ , for the both the unloaded and loaded cases is computed by:

$$I = A \times |A|. \quad (\text{S1})$$

We compute the mean OCT intensity,  $\mu_I$ , in the complex domain:

$$\mu_I = \frac{1}{N} \sum_{j=1}^N I_j. \quad (\text{S2})$$

The mean complex OCT intensity is converted back to mean complex OCT amplitude,  $\mu_A$ , by:

$$\mu_A = \frac{\mu_I}{\sqrt{|\mu_I|}}. \quad (\text{S3})$$

The mean OCT amplitude is found by taking the absolute value of Eq. (S3). Speckle brightness in Section 4 is computed using the unloaded mean OCT amplitude.

To determine the OCT SNR for a given B-scan, firstly, the standard deviation,  $\sigma$ , inside a region containing no signal in the mean complex OCT amplitude is computed for both cases. The linear OCT SNR ( $SNR_{linear}$ ) is then computed by:

$$SNR_{linear} = \left| \frac{\mu_A}{\sigma} \right|^2. \quad (S4)$$

The OCT SNR in decibels (dB) ( $SNR_{dB}$ ) is given by:

$$SNR_{dB} = 10 \times \log_{10} (SNR_{linear}). \quad (S5)$$

We present the unloaded OCT SNR in dB in Section 4.

To compute the mean phase difference, we first compute the phase difference between the unloaded ( $A_{UL}$ ) and loaded ( $A_L$ ) complex OCT amplitude B-scans in each B-scan pair. We then compute the mean in the complex domain, where the mean phase difference ( $\mu_{\Delta\phi}$ ) B-scan is given by:

$$\mu_{\Delta\phi} = \angle \frac{1}{N} \sum_{j=1}^N A_{L_j} \times \overline{A_{UL_j}}. \quad (S6)$$

where  $\overline{A}$  represents the complex conjugate of  $A$ .

In Section 4, the corresponding strain B-scans are computed from the mean phase difference B-scans given by Eq. (S6).

## References

1. B. H. Park, M. C. Pierce, B. Cense, S.-H. Yun, M. Mujat, G. J. Tearney, B. E. Bouma, and J. F. de Boer, "Real-time fiber-based multi-functional spectral-domain optical coherence tomography at 1.3  $\mu\text{m}$ ," Opt. Express **13**(11), 3931–3944 (2005).
2. J. W. Goodman, *Statistical Optics* (John Wiley & Sons, 2015).
3. S. Makita, F. Jaillon, I. Jahan, and Y. Yasuno, "Noise statistics of phase-resolved optical coherence tomography imaging: single-and dual-beam-scan Doppler optical coherence tomography," Opt. Express **22**(4), 4830–4848 (2014).